Preprints of the 21st IFAC World Congress (Virtual)
Berlin, Germany, July 12-17, 2020

Robust and Reliable Multi-Sensor Navigation Filter for Maritime Application

J.J. Gehrt * **S. Liu** * **M. Nitsch** * **W. Bruhn** ** **S. Rohde** **
R. Zweigel * **D. Abel** *

* *Institute of Automatic Control, RWTH Aachen University, Germany (e-mail: j.gehrt@ irt.rwth-aachen.de).*
** *Raytheon Anschütz GmbH, Kiel, Germany (e-mail: wilko.bruhn@raytheon.com).*

Abstract: This publication describes the further development of a navigation concept especially designed for maritime application and its recent integration on the research ship DENEB of the German Federal Maritime and Hydrographic Agency (BSH). The proposed navigation concept consists of a tightly-coupled navigation filter, which bases on quantities of an inertial measurement unit (IMU), is aided by a Doppler velocity log (DVL), and Global Navigation Satellite System (GNSS) dual constellation signals of two antennas. Integrity monitoring with fault detection and exclusion (FDE), ensures the reliability of the GNSS observables. A new approach for integrating low quality and biased DVL data without endangering the state estimation accuracy and preciseness, but enhancing it's robustness is introduced. A new integration of real-time sea level data from an online service in the filter improves robustness in addition. The navigation system is evaluated in an extensive measurement campaign with DENEB in harbor of Rostock, Germany. Basically, two different advantages of the proposed navigation concept are investigated. Firstly, evaluation proves that integration of the low quality and biased data of the vessels DVL is possible without lowering the navigation filter accuracy significantly. Secondly, the robustness of the concept against sensor failure is shown. Therefore, by means of post-processing the recorded data, GNSS and DVL outage is investigated. Evaluation verifies, that the multi-sensor fusion and the integration of real-time sea level data improves the robustness of the navigation solution and therefore is qualified for autonomous application.

Keywords: Autonomous vehicles, Global positioning systems, Inertial navigation, Kalman filters, Multisensor integration, Navigation systems, Sensorfusion

1. INTRODUCTION

In the area of mobility, satellite-based navigation provides a substantial contribution to future innovation and to the ongoing shift towards automated vehicles. European Global Navigation Satellite System Agency (2019) states that the future of ships is autonomous. Herein, an overview of main user requirements in maritime says that, especially for port operations, availability, integrity and sub meter accuracy is required. In order to provide a robust and reliable GNSS-based navigation system for maritime applications, the influence of ever-changing disturbances must be compensated, e.g. satellite signal shadowing and reflection within harbors, onboard sensor failures and loss of connection to ground based augmentation service (GBAS). As a solution of these challenges, a concept is proposed, which couples inertial measurements, satellite observables from multiple antennas and GBAS, together with accurate velocity data and environmental data from external services. The questions remain, how to apply such approach to an existing vessel and how to integrate sensors of the vessels own to realize this concept.

The present publication bases on previous works. In Gehrt et al. (2018) a tightly-coupled navigation filter is introduced. This navigation filter bases on IMU quantities and is aided by GNSS observables, pseudoranges and deltaranges, from the Galileo and GPS system. A DVL is utilized, which improves the navigation filter accuracy in case of low GNSS signal quality, and ensures the filter robustness in case of small amount of available satellites, or even total GNSS failure. For parameterization of the DVL measurement noise in the navigation filter, the figure of merrit (FOM), directly provided by the DVL, is used. In order to achieve accurate fusion, DVL measurement delay is estimated, by using GNSS digital trigger, the so called pulse per second (PPS), and the estimated supersonic signal travel time in water, provided by the DVL. However, transferring the navigation filter to real vessels, requires the algorithms to deal with NMEA message format used on vessels communication network and data of probably lower quality. In the current work, the access to the vessels navigation NMEA messages is performed by the Raytheon Anschütz bridge software SYNAPSIS. In order to deal with low quality measurements, DVL bias states are introduced to the navigation filter.

Integration of height information in the sensor fusion is widely investigated. I.e. Gädeke et al. (2012) introduces integration of barometer measurements to aid the height

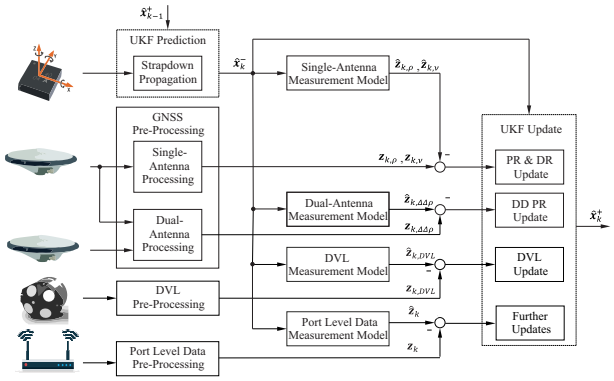

Fig. 1. Block diagram of the navigation filter, providing measurement models and associated update steps.

estimation. In Gehrt et al. (2017) an approach is introduced, which adds an artificial height update together with an height change assumption to a navigation filter. In the present work this approach is adapted, to fuse online sea level data from an external service within the navigation filter. For this purpose, a client for external services is introduced. Besides the sea level data, it delivers GBAS observables from a reference station in RTCM format.
Integrity monitoring protects satellite-based navigation systems against possible GNSS measurement faults. For this purpose, Pervan et al. (1996) applies receiver autonomous integrity monitoring (RAIM) approach with parity space for single GPS fault identification. The previous work Liu et al. (2019) extends this approach to dual constellation application and studies the accuracy improvement by using RAIM. Additionally, a fault exclusion scheme is proposed, specially for maritime applications. However, integrating integrity monitoring in a multi-sensor navigation filter running on a real vessel, has not been investigated yet. Therefore, in current presentation, the mentioned integrity system is validated with data recorded on a real vessel.
This paper is structured as follows: First, in Sec. 2, basic ideas of the tightly-coupled navigation filter are explained, followed by a description of filter extensions for additional DVL measurements and port level data. Further, GNSS integrity monitoring is explained briefly. Sec. 3 provides the measurement setup and target hardware, including the integration of SYNAPSIS bridge. Experimental results are presented and discussed at the end of this paper.

2. METHODOLOGY

2.1 Navigation Filter

The navigation filter scheme is shown in Fig. 1. It makes use of an unscented Kalman (UKF) update, which fuses information from several sensor systems with a rate of 100 Hz. These include an IMU, two GNSS receivers, each with corresponding antenna, a DVL and external data services, providing harbor sea level data. Data from all sensor system gets pre-processed before being fed into filter. The navigation filter provides four measurement update steps, based on four measurement models. IMU data is integrated as process model within UKF prediction step using the well-known strapdown algorithm. Within the navigation filter, a 6-DOF nonlinear state-space model in continuous form is used:

$$\dot{\boldsymbol{x}} = \boldsymbol{f}(\boldsymbol{x}, \boldsymbol{u}) + \boldsymbol{G}\boldsymbol{w}, \qquad \boldsymbol{w} \sim \mathcal{N}(0, \boldsymbol{Q}) \tag{1}$$
$$\boldsymbol{z} = \boldsymbol{h}(\boldsymbol{x}) + \boldsymbol{v}, \qquad \boldsymbol{v} \sim \mathcal{N}(0, \boldsymbol{R}) \tag{2}$$

where the state of the system is denoted by $\boldsymbol{x}$. $\boldsymbol{w}$ is the process noise, $\boldsymbol{v}$ describes measurement noise. Both noise sources are modeled by zero-mean Gaussian distributions using covariance matrices $\boldsymbol{Q}$ and $\boldsymbol{R}$. $\boldsymbol{f}(\boldsymbol{x}, \boldsymbol{u})$ and $\boldsymbol{h}(\boldsymbol{x})$ represent the continuous nonlinear state transition and measurement model. $\boldsymbol{G}$ is the continuous noise shaping matrix. The state vector $\boldsymbol{x}$ is composed of position $\boldsymbol{p}^e_{eb}$ of the IMU body frame origin in Earth-Centered-Earth-Fixed (ECEF) coordinates (3×1), velocity $\boldsymbol{v}^n_{eb}$ in navigation frame North-East-Down (NED) coordinates (3×1), a quaternion $\boldsymbol{q}^n_b$ for alignment of body frame and NED frame (4×1) and accelerometer bias $\boldsymbol{b}_a$ and gyroscope bias $\boldsymbol{b}_g$, each of dimension (3×1). Additionally, a tightly coupled system needs to estimate receiver clock bias c_b and drift c_d for correction of pseudo- and deltaranges. Therefore, the state vector $\boldsymbol{x} = [\boldsymbol{p}^e_{eb}\ \boldsymbol{v}^n_{eb}\ \boldsymbol{q}^n_b\ \boldsymbol{b}_a\ \boldsymbol{b}_g\ c_b\ c_d]^T$ is of dimension 18. The observability of navigation systems consisting of an IMU and a position sensor has been studied in Batista et al. (2011). It is shown, that observability of bias states is given, if driven trajectories are rich enough. For the present publication it is assumed that observability of all bias states is given as long as a sufficient geometrical constellation of satellites is given.

Process Model Considering the nonlinear process model in Eq. (1), the state transition model $\boldsymbol{f}(\boldsymbol{x}, \boldsymbol{u})$ bases on the strapdown mechanization, which calculates position, velocity and attitude, given measured acceleration and angular rate, summed up in the input vector $\boldsymbol{u}$. The algorithm can be found in Farrell (2008). Accelerometer and gyroscope bias are estimated using a random-walk model as proposed by Petovello (2003). The clock error estimation bases on a first-order Gauss-Markov model. The process covariance matrix parameterization bases on IMU Allan Variance analysis as presented by the publication Breuer et al. (2016).

Single- and Dual-Antenna Measurement Model As shown in Fig. 1, GNSS data gets pre-processed before used in further calculations within the measurement models. The applied pre-processing, the single-antenna measurement model using pseudo- and deltaranges, the dual-antenna measurement model using double-differenced pseudoranges and parameterization of corresponding covariance matrices can be found in the related publication Gehrt et al. (2019).

DVL Measurement Model The integration of DVL measurements in an extended Kalman filter, with direct access to DVL raw data, was introduced in Gehrt et al. (2018). In the present publication, DENEB only provides the NMEA VBW message, which results in significantly disadvantages:

- No velocity in z-direction of the DVL body frame.
- Worse quality of the velocity measurement.
- Maximum velocity resolution of 0.1 kn.
- No possibility to trigger the DVL measurement in order to estimate the measurement delay.
- No information about measurement quality.

For implementation of the DENEB DVL in the existing navigation filter, it is assumed that the velocity in z-direction of the body frame equals zero; x- and y-velocity

are taken directly from the NMEA VBW message. The resulting measurement is:

$$\tilde{\boldsymbol{z}}_{DVL} = \begin{pmatrix} \text{VBW: Longitudinal ground speed} \\ \text{VBW: Transverse ground speed} \\ 0 \end{pmatrix} \quad (3)$$

Including the low quality DENEB DVL data in the measurement model from Gehrt et al. (2018) just like it is, would mean to lower the resulting navigation filter state estimation accuracy. To face this challenge, the idea is to add additional degree of freedom, by introducing measurement bias errors for the x- and the y-velocity in the DVL body frame to the measurement model.
Therefore, two new temporally states $b_{x,DVL}$ and $b_{y,DVL}$ are introduced to the state vector in Eq. (2.1). Both are modeled as random walk, which adds the following equation to the process model:

$$\dot{\boldsymbol{b}}_{DVL} = \boldsymbol{0} + \boldsymbol{I}_{2\times 2} \times \boldsymbol{w}_{DVL} \ , \quad (4)$$

where a small constant noise for both biases of 0.1 $\frac{m}{s}$ for achieving stiff dynamic behavior is assumed. $\boldsymbol{b}_{DVL}$ is called temporally state, because it is only propagated and corrected, as long as GNSS measurements are available. This approach ensures that the relationship between confidence in the DVL measurement and confidence in the predicted measurement does not develop too strongly in the direction of the measurement, during phases of GNSS outage.
The resulting DVL measurement equation for the UKF update is:

$$\hat{\boldsymbol{z}}_{DVL} = \boldsymbol{C}_b^{b,DVL}\left[\boldsymbol{C}_n^b \boldsymbol{v}_{eb}^n + \boldsymbol{w}_{ib}^b \times \boldsymbol{l}_{DVL}^b\right] + \boldsymbol{b}_{DVL} + \boldsymbol{v}_{DVL},\ \boldsymbol{v}_{DVL} \sim \mathcal{N}(0, \boldsymbol{R}_{DVL}) \ , \quad (5)$$

where $\hat{\boldsymbol{z}}_{DVL}$ is the estimated DVL measurement, which is the velocity of the DVL body frame relative to the ECEF frame in the DVL body frame coordinates. $\boldsymbol{C}_n^b$ is the inverse of $\boldsymbol{C}_b^n$ and rotates the estimated DVL velocity from NED frame to the DVL body frame. $\boldsymbol{C}_b^{b,DVL}$ rotates the IMU body frame in the DVL body frame. It equals the identity, with the assumption, that the IMU body frame (b) and the DVL body frame (b,DVL) have the same orientation. $\boldsymbol{l}_{DVL}^b$ is the lever arm pointing from the IMU body frame to the DVL body frame in IMU body frame coordinates. $\boldsymbol{v}_{DVL}$ is the measurement noise. Since measurement quality information like figure of merrit (FOM) is not available, the standard deviation of $\boldsymbol{v}_{DVL}$ is parameterized with respect to the mean estimates in Gehrt et al. (2018) as constant 0.1 m/s.

Sea Level Data Measurement Model Port level data is integrated in the navigation filter as an additional virtual satellite. Here, the virtual satellite has its position in the WGS84 ellipsoid center and has a zero velocity. The virtual satellite deltarange equals zero and the corresponding measured pseudorange $\tilde{z}_{sl}$ is modeled on the basis of the dynamic port level information as follows:

$$\tilde{z}_{sl} = r_{WGS84}^e(\boldsymbol{p}_{eb}^e) + h_{sl}^e + \delta h_{sl}^b + l_{z,Ant}^b + v_{sl}^b \ . \quad (6)$$

Here, $r_{WGS84}^e(\boldsymbol{p}_{eb}^e)$ is the radius from the center of the WGS84 ellipsoid to the current position $\boldsymbol{p}_{eb}^e$. h_{sl}^e is the height of the sea level in the ECEF frame. δh_{sl}^b is the difference of the mounted height of the IMU relative to keel and the vessels draught, calculated from the vessels general plan. $l_{z,Ant}^b$ is the z-component of the lever arm of the antenna and adds the height difference between IMU and antenna. Both, δh_{sl}^b and $l_{z,Ant}^b$ are modeled independent from roll and pitch, since it is assumed, that roll and pitch are small in the harbor area. All uncertainties are summarized in v_{sl}^b.
Real-time port level data can be assessed from a network of measurement stations of the German Federal Waterways and Shipping Authority in elevation network SNN76. With respect to the own position, the closest measurement point has to be chosen first. Meta data and the current time variant sea level h_{sl}^{PNP} relative to the local zero point (PNP) can be received from an online service. The meta data consists of the information δh_{PNP}^{SNN76}, which is the difference between PNP and the elevation network in SNN76. In order to integrate the sea level in the navigation filter it must be transferred into the WGS84 frame, such that it is formulated in the ECEF frame as follows:

$$h_{sl}^e = h_{sl}^{PNP} + \delta h_{PNP}^{SNN76} + \delta h_{SNN76}^{DHHN92} + h_{und} + v_{sl}^{PNP} \ , \quad (7)$$

where $\delta h_{SNN76}^{DHHN92}$ shifts the height relations to the DHHN92 elevation network, which enables the calculation of undulation h_{und}, in order to transfer the sea level to geoid understanding of WGS84. $\delta h_{SNN76}^{DHHN92}$ and h_{und} are calculated by means of maps from the German Federal Agency of Cartography and Geodesy and requires the position of the sea level measurement point $\boldsymbol{p}_{mp}$ as input.
Finally, the associated measurement model for the Kalman filter is obtained in the form of

$$\begin{pmatrix} \hat{z}_{\rho,sl} \\ \hat{z}_{v,sl} \end{pmatrix} = \begin{pmatrix} \|[0\ 0\ 0] - \boldsymbol{p}_{e|Ant}^n\|_2 \\ (\boldsymbol{e}_{e|Sat}^n)^T([0\ 0\ 0] - \boldsymbol{v}_{e|Ant}^n) \end{pmatrix} + \begin{pmatrix} v_{\rho,sl} \\ v_{v,sl} \end{pmatrix} \quad (8)$$

where $v_{\rho,sl}$ is the noise of the artificial pseudorange and takes account of v_{sl}^b and v_{sl}^{PNP} for the artificial pseudorange, respectively the altitude. $v_{v,sl}$ is the noise of the artificial deltarange. Here, the sea waves on which the ships move up and down are modeled as Gaussian noise. For the harbor environment it is assumed, that the standard deviation of the altitude measurement is 1 m and the standard deviation of the altitude velocity is 0.5 m.

2.2 GNSS Integrity Monitoring

RAIM is used for fault detection and identification as introduced in Liu et al. (2019). RAIM predicts pseudorange residual vector $\boldsymbol{r}_s$, which is based on estimated vehicle position using least square method, and uses the residuals to detect and identify pseudorange faults. According to statistics, with ν independent standard normal random variables, the sum of their squares satisfies ν degree of freedom (DOF) chi-squared distribution. Assuming that the pseudorange measurement noise satisfies the white mean Gaussian distribution with various standard deviation. After using pseudorange measurements to estimate the unknowns by using least square approach, the normalized predicted residual of pseudoranges ν shall satisfy $N-4$ DOF chi-squared distribution. Otherwise, RAIM shall declare that an error occurred.
The fault identification is done iteratively, with the help of parity space using Bayes Rule, assuming all satellites having the same prior probability of being faulty. The satellite corresponds to the highest possibility is considered to contain the faulty measurement. The identified faulty measurement is isolated from the GNSS measurements at first. Then, fault detection and identification are repeated

with the rest of measurements, until there is no fault alert or no faulty measurements can be identified. With the fault exclusion scheme introduced in Liu et al. (2019), the identified faulty measurements are excluded for a certain duration and the minimum number of satellites is guaranteed, for a robust and smooth navigation estimation.

3. EXPERIMENTAL VALIDATION

3.1 Test Vessel DENEB and Bridge Software SYNAPSIS

The presented navigation filter should be evaluated and validated under operational conditions in an industrially relevant environment. For this purpose, the research ship DENEB serves as an experimental vehicle. DENEB acts as a carrier for Raytheon Anschütz SYNAPSIS software for intelligent bridge control. This state-of-the-art INS (Integrated Navigation System) interfaces shipboard sensors systems and actuator control systems and thus serves as a platform for advanced applications for ship automation. As part of its standard features, SYNAPSIS provides e.g. consistent sensor data management. A respective full-scale navigation bridge is installed in a mobile 10' offshore container and positioned on board of the research ship. Shipboard data exchange is implemented in compliance with NMEA 0183 Standard for interfacing marine electronic devices to facilitate post-project exploitation. This interface provides the NMEA VBW DVL bottom track velocity, used in Sec. 2.1.3.

3.2 Navigation Filter Experimental Setup

Fig. 2 shows the navigation filter measurement setup on DENEB. Septentrio PolaNt-x MF antennas are mounted at the top deck of DENEB. A LORD MicroStrain 3DM-GX4-25 industrial-class IMU sensor is placed in the bridge. The vessels DVL used in this experiment places near the thruster bow. These result in following lever arms:

$$\boldsymbol{l}^b_{Ant1} = [3.300, \quad 2.294, \quad -4.775]^T, \tag{9}$$

$$\boldsymbol{l}^b_{Ant2} = [3.300, \quad -3.480, \quad -4.825]^T, \tag{10}$$

$$\boldsymbol{l}^b_{DVL} = [23.650, \quad 0, \quad 10.175]^T, \tag{11}$$

Antenna one (subscript Ant1) is used for the basic single antenna filter update and antenna two, together with antenna one for the double difference dual antenna filter update. For processing, the setup consists of a dSPACE MicroAutoBox II and a Rapid Control Prototyping (RCP) unit. Two Septentrio AsteRx3 receivers are utilized for receiving the required individual GNSS observables from the two antennas. For reference purposes, the Real Time Kinematic (RTK) solution from the first receiver is used. A Raspberry Pi serves as client for external data support. RTCM messages are received, processed and forwarded to the dSPACE MicroAutoBox II for GNSS observable correction. *pegelonline.wsv.de* is accessed by the same Raspberry Pi. The meta data of the closest measurement point as well, as its real-time sea level data is decoded with a HTML-parser and send to the dSPACE MicroAutoBox II.

3.3 Experimental Results

Evaluation Scenario For the following evaluations a docking scenario is chosen. First subfigure in Fig. 3 shows

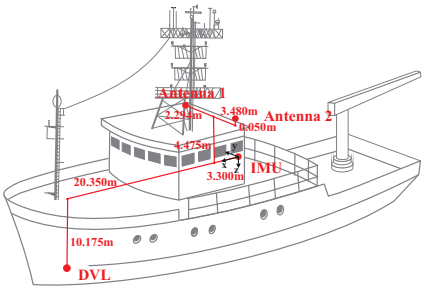

Fig. 2. Sketch of sensor distribution and IMU-body frame on the experiment ship DENEB: IMU, DVL and 2 GNSS antennas.

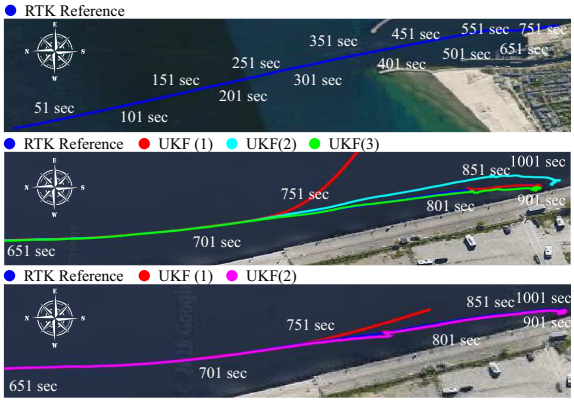

Fig. 3. 2D driven trajectory of the DENEB entering the port of Rostock, Germany and the subsequent docking maneuver. first subfigure: RTK reference. Second (for Sec. 3.3.2) and third subfigure (for Sec. 3.3.3): detail of GNSS failure phase just before docking. Map Data: ©2019 GeoBasis/BKG(©2009), Google.

the corresponding RTK reference trajectory of DENEB entering the harbor of Rostock, Germany and subsequently docking. Timestamps correspond to those of all other evaluation figures, in order to enable better comparison. Data during testing is recorded to enable post-processing of different navigation filter configurations later.

Evaluation DVL Integration The functionality of the DENEB DVL integration and the enhancement of introducing the DVL bias states in terms of robustness is validated by evaluating different UKF configurations for a GNSS failure event, where all satellites are lost. Until this event GNSS single-antenna GPS L1 observables corrected by differential data and for the dual-antenna update dual-constellation observables of GPS and Galileo satellites are utilized. This configuration is chosen, in order to achieve the highest possible state estimation accuracy. Furthermore, the three following different filter settings are investigated:

(1) UKF with dual-antenna aiding but without DVL integration, in order to show the drift of the states when only IMU propagation is done.
(2) UKF with dual-antenna and DVL aiding, but without the additional DVL bias states, in order to show the resulting lower accuracy of state estimation.
(3) UKF with dual-antenna and DVL aiding and the additional DVL bias states, in order to show the accuracy enhancement in phases where GNSS is

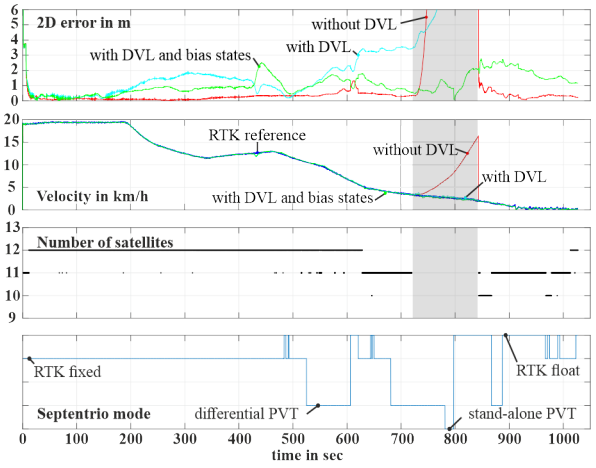

Fig. 4. Evaluation: Comparison of UKF configuration 1) (red), 2) (cyan) and 3) (green) and RTK reference (blue).

available and the robustness enhancement in phase of GNSS failure.

Second subfigure in Fig. 3 provides a detail of the driven trajectories with the three different UKF configurations. That corresponds to the first plot of Fig. 4, which shows the 2D error, which is the Euclidean distance between the RTK reference and each UKF configuration. The second plot of Fig. 4 shows the estimated absolute velocity of all three configurations and the velocity of the RTK reference system. The plot below, visualizes the number of available satellites along the test and shows directly the phase of GNSS failure, which is marked by the gray background for all other plots. The last plot of this figure provides the reference receiver mode. It says, that not all the time a reliable position reference and therefore reliable 2D error calculation is possible, since not all the time the receiver is in RTK fixed mode. Taking both figures Fig. 3 and Fig. 4 into account, obviously, the position solution of the configuration without DVL aiding at all (red) shows highest accuracy in phases of GNSS availability. Before entering the harbor the 2D error is below 20 cm. After entering the harbor the accuracy becomes a little lower but is still under 50 cm, due to harbor infrastructure influencing the signal quality (see Sec. 3.3.4). But when GNSS failure at second 720 happens, it drifts rapidly away. In comparison, the configuration with DVL but without DVL bias estimation (cyan) performs better on GNSS failure, but including the DVL in the UKF results in a significantly lower position accuracy. The configuration with DVL and the introduced DVL bias estimation (green) still is of lower accuracy than configuration (1), but is mostly still below 1 m. However, obviously it shows best behavior after GNSS loss. Fig. 5 compares the actual DVL measurement $\tilde{\boldsymbol{z}}_{DVL}$ with the predicted measurement $\hat{\boldsymbol{z}}_{DVL}$ in case of the standard UKF with 18 states (blue) and in case that the UKF estimates a DVL measurement bias $\boldsymbol{b}_{DVL}$ (green) in addition. The blue evaluation shows what the highly accurate UKF estimation expects to get from DVL. Especially before entering the harbor, DENEB drifts along the body frame y-axis, but the DVL is not able to provide this information. This is the reason, why the UKF with DVL aiding but without additional DVL biases performs that bad. Introducing the

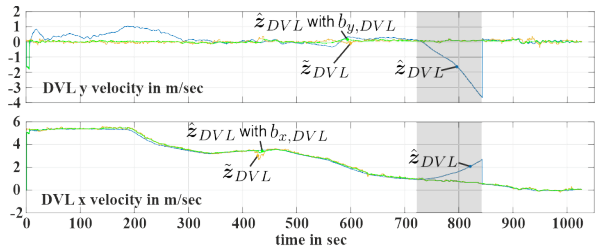

Fig. 5. Evaluation: Comparison of measured (orange) and predicted DVL velocity, with (green) and without (blue) bias states in the measurement model.

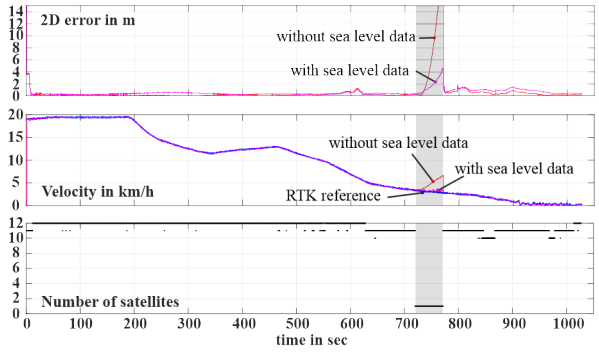

Fig. 6. Evaluation: Comparison of configuration UKF 1) (red) and 2) (magenta) and RTK reference (blue).

dynamic bias estimation mitigates the DVLs bad influence. It should be noted that introducing the biases only works, as long the dynamics of the vessel are low and the direction of motion during GNSS failure does not change rapidly.

Evaluation Sea Level Data Integration The functionality of the sea level data integration and the enhancement of robustness is validated by evaluating the same docking scenario like in Sec. 3.3.2. But instead of total GNSS failure (gray marked phase in Fig. 6), here two satellites (G02 and G19) of low elevation angle and similar azimuth (west relative to ship position) remain in order to demonstrate the capability of sea level data to aid the state estimation. Until this event GNSS single-antenna aiding GPS L1 observables corrected by differential data are used. Orientation aiding with the dual-antenna approach is not applied. Furthermore, the following filter settings are investigated:

(1) UKF with dual-antenna aiding but without sea level data integration, in order to show the drift of states when propagation is aided by the two satellites only.
(2) UKF with dual-antenna sea level data aiding, in order to show the improvement of state estimation, due to the better geometrical constellation of the available ranging sources, after adding the virtual sea level data satellite.

Third subfigure in Fig. 3 and Fig. 6 show the same evaluations as Fig. 3 and Fig. 4 but with the sea level data aiding UKF configurations. The reference receiver mode evaluation stays the same and is therefore not repeated. Both figures show the significant better performance of the sea level aided configuration, when only two satellites are available. G02 and G19 together build a very unfavorable geometrical constellation. Adding the sea level data as additional ranging source pointing from the center of

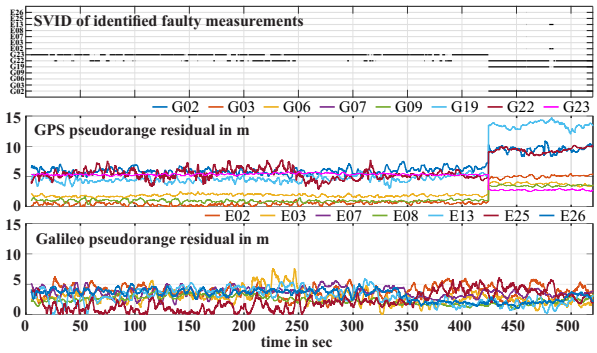

Fig. 7. Evaluation of integrity system: first subfigure: results of fault identification; second and third pseudorange residuals during the drive

Earth to antenna 1 improves the geometrical constellation significantly in this case. Therefore, the drift of the position estimation with sea level data aiding is mitigated significantly and the drift of velocity estimation is nearly totally eliminated.

Evaluation Integrity The FDE functionality of the GNSS integrity module is validated by checking the correlation of fault identification results with pseudorange residuals during the drive. The pseudorange residuals are calculated as the difference between measured and true pseudoranges. Here, true pseudoranges are estimated with the high accurate RTK reference solution and satellites position. Therefore, this validation can only be carried out, when RTK fix solution is available, i.e. until second 520 in this experiment. The first subfigure in Fig. 7 shows the results of the fault identification. The results can be divided into two parts: Phase I is from the beginning till second 420, when the ship drives outside the harbor; Phase II is after second 420, when the ship enters the harbor. In Phase I, only two GPS satellites, G22 and G23, are identified as faulty, mainly G23. The second and third subfigure in Fig. 7 shows that, G22 and G23 certainly have one of the largest residuals. However, their residuals are not much larger than G02 and G09. The reason G22 and G23 are identified as faulty is that they have relatively higher elevation, resulting in larger horizontal positioning error. In Phase II, G02, G19 and G22 are mainly identified as faulty. This can also be validated by the second and third subfigure. In this phase, the residuals of those three satellite are significantly larger than others.

4. CONCLUSION

The present work introduces technical developments of an existing tightly-coupled navigation filter for application on the research ship DENEB, aiming for highly reliable state estimation. Discussion of results confirm, that DVL as well as sea level data improves robustness and can aid state estimation in phases of restricted satellite visibility or total GNSS loss. But it shows as well, that including lower quality sensor data, containing unpredictable biases, lowers total state estimation accuracy. Introducing bias states for the low quality DVL mitigates this behavior and fits for the current application of low dynamic maneuvering. Future work will further improve the accuracy of navigation solution by introducing GNSS carrier phase measurements into the navigation filter. Moreover, the future development may concentrate more on integrity monitoring of all fused measurements and protection level estimation for multi-sensor integrated navigation filters.

ACKNOWLEDGEMENTS

The joint research project GALILEOnautic 2 is supported by the German Federal Ministry for Economic Affairs and Energy (grant 50NA1808). Basis for the support is a decision by the German Bundestag.

REFERENCES

Batista, P., Silvestre, C., and Oliveira, P. (2011). On the observability of linear motion quantities in navigation systems. *Systems & Control Letters*, 60(2), 101–110. doi:10.1016/j.sysconle.2010.11.002.

Breuer, M., Konrad, T., and Abel, D. (2016). High Precision Localisation in Customised GNSS Receiver for Railway Applications. In *Proceedings of the 29th International Technical Meeting of The Satellite Division of the Institute of Navigation (ION GNSS+ 2016)*, 779–787. Portland, Oregon.

European Global Navigation Satellite System Agency (2019). *GSA GNSS Market Report 2019*. Publications Office of the European Union.

Farrell, J. (2008). *Aided navigation : GPS with high rate sensors*. New York : McGraw-Hill. Formerly CIP.

Gädeke, T., Schmid, J., Zahnlecker, M., Stork, W., and Muüller-Glaser, K.D. (2012). Smartphone Pedestrian Navigation by Foot-IMU Sensor Fusion. In *Proceedings of 2012 Ubiquitous Positioning, Indoor Navigation, and Location Based Service (UPINLBS)*. IEEE.

Gehrt, J.J., Breuer, M., Konrad, T., and Abel, D. (2017). A pseudolite position solution within a Galileo test environment for automated vehicle applications. In *2017 European Navigation Conference (ENC)*, 135–142. doi: 10.1109/EURONAV.2017.7954202.

Gehrt, J.J., Zweigel, R., Konrad, T., and Abel, D. (2018). DVL-aided Navigation Filter for Maritime Applications. *IFAC-PapersOnLine*, 51(29), 418 – 423. doi: https://doi.org/10.1016/j.ifacol.2018.09.451. 11th IFAC Conference on Control Applications in Marine Systems, Robotics, and Vehicles CAMS 2018.

Gehrt, J.J., Nitsch, M., Abel, D., and Zweigel, R. (2019). High accuracy navigation filter with dual antenna enabling double-differencing with dual-constellation. In *Proceedings of the 32nd International Technical Meeting of the Satellite Division of The Institute of Navigation (ION GNSS+ 2019)*.

Liu, S., Gehrt, J.J., Abel, D., and Zweigel, R. (2019). Dual-constellation aided high integrity and high accuracy navigation filter for maritime applications. In *Proceedings of the 2019 International Technical Meeting of The Institute of Navigation*, 762–774.

Pervan, B., Lawrence, D., Cohen, C., and Parkinson, B. (1996). Parity space methods for autonomous fault detection and exclusion using gps carrier phase. *Position Location and Navigation Symposium*, 649–656.

Petovello, M. (2003). *Real-time integration of a tactical-grade IMU and GPS for high-accuracy positioning and navigation*. Citeseer.